JPE 18-3-14

https://doi.org/10.6113/JPE.2018.18.3.789
ISSN(Print): 1598-2092 / ISSN(Online): 2093-4718

Model Predictive Power Control of a PWM Rectifier for Electromagnetic Transmitters

Jialin Zhang†, Yiming Zhang*, Bing Guo*, and Junxia Gao*

†,*Faculty of Information, Beijing University of Technology, Beijing, China

Abstract

Model predictive direct power control (MPDPC) is a widely recognized high-performance control strategy for a three-phase grid-connected pulse width modulation (PWM) rectifier. Unlike those of conventional grid-connected PWM rectifiers, the active and reactive powers of permanent magnet synchronous generator (PMSG)-connected PWM rectifiers, which are used in electromagnetic transmitters, cannot be calculated as the product of voltage and current because the back electromotive force (EMF) of the generator cannot be measured directly. In this study, the predictive power model of the rectifier is obtained by analyzing the relationship among flux, back EMF, active/reactive power, converter voltage, and stator current of the generator. The concept of duty cycle control in the proposed MPDPC is introduced by allocating a fraction of the control period for a nonzero vector and rest time for a zero vector. When nonzero vectors and their duration in the predefined cost function are simultaneously evaluated, the global power ripple minimization is obtained. Simulation and experimental results prove that the proposed MPDPC strategy with duty cycle control for the PMSG-connected PWM rectifier can achieve better control performance than the conventional MPDPC-SVM with grid-connected PWM rectifier.

Key words: Direct power control, Electromagnetic transmitter, Model predictive control, Permanent magnet synchronous generator

I. INTRODUCTION

Electromagnetic transmitters are essential parts of an electromagnetic exploration system. They reverse the steady power supply at a desired frequency and transmit power via grounding electrodes to obtain an effective electromagnetic field for deep geophysical exploration. To acquire geophysical data during deep exploration and meet field operation requirements, these transmitters should exhibit good anti-interference capability and high power density with high-accuracy output while remaining compact and light.

The topology and control methods of the power supply for geophysical exploration have been widely studied [1]-[5]. In [1], an AC/DC/AC topology is proposed (Fig. 1), in which the inverter circuit is directly connected with a three-phase, six-pulse diode rectifier. Although the structure of the transmitter is simple, the output voltage is low. In [2]-[4], an AC/DC/AC/DC/AC structure is designed with variable output voltage and a simple controller, thereby offering easy implementation and high universality. In [2], [3], a hard-switching DC/DC converter is adopted (Fig. 2). In [2], a triple-loop control with GAPSO algorithm is established. In [3], an air-cooling system is designed and its loss is analyzed. In [4], an active full bridge soft switching DC/DC converter is employed (Fig. 3). However, the double DC/DC converter adds complexity to the system structure, and the inductance and transformer increase the volume and weight. In [5], an excitation control method is provided to regulate the output voltage in an AC/DC/AC topology. The transmitter is simple in structure, small in volume, and light in weight because of the absence of the inductance and transformer. However, when the generator runs in a nonlinear part, the excitation is difficult to control. The three-phase diode used for electromagnetic transmitters exhibit simplicity, robustness, and cost efficiency. However, the diode rectifier results in a unidirectional flow of power, low input power factor, and high input current harmonics. In the present study, a pulse width modulation (PWM) rectifier for electromagnetic transmitter is designed. Different from those of a conventional PWM rectifier, the external inductances of the proposed rectifier are replaced by the armature inductance of the generator (Fig. 5).

Manuscript received Aug. 16, 2017; accepted Feb. 3, 2018
Recommended for publication by Associate Editor Il-Oun Lee.
†Corresponding Author: zhangjialin373@126.com
Tel: +86-10-6739-6621, Fax: +86-10-6739-6621, Beijing Univ. of Tech.
*Faculty of Information, Beijing University of Technology, China

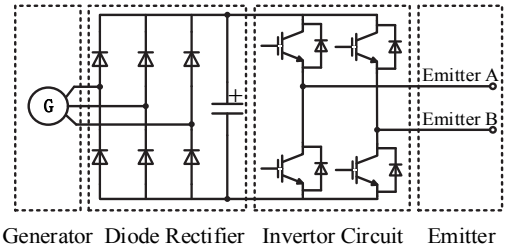

Fig. 1. Topology of a conventional transmitter with a diode rectifier.

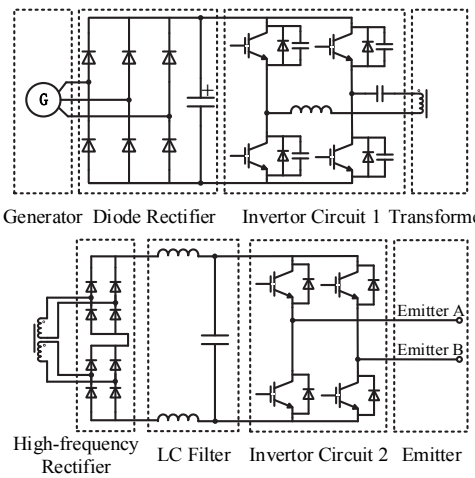

Fig. 2. Topology of a conventional transmitter with a hard-switching DC/DC converter.

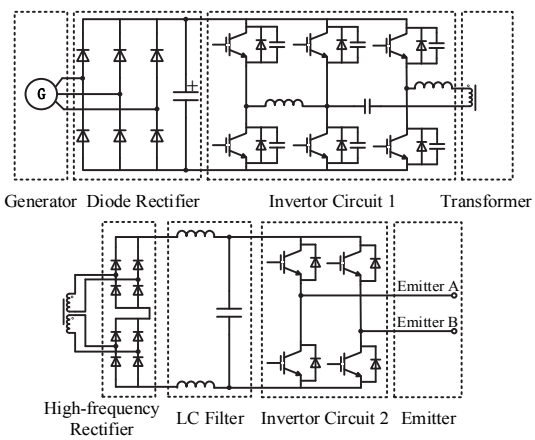

Fig. 3. Topology of a conventional transmitter with an active full-bridge soft-switching DC/DC converter.

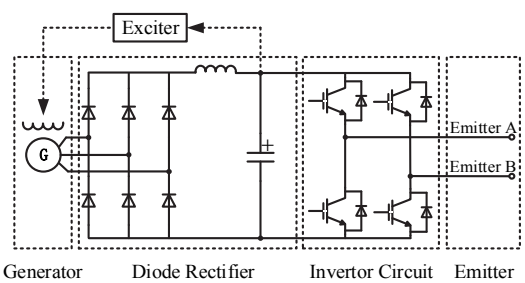

Fig. 4. Topology of a conventional transmitter with excitation control.

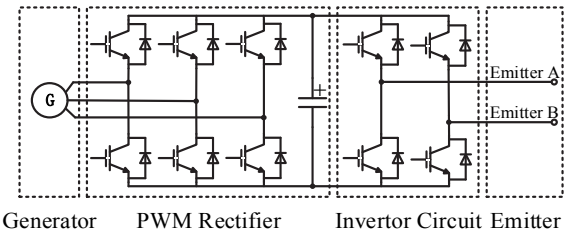

Fig. 5. Topology of the proposed transmitter.

PWM rectifiers are adopted in industrial applications because of certain advantages, such as bidirectional power flow, low harmonic distortion of line current, unit power factor operation, and adjustment and stabilization of the DC-link voltage. In addition, the size of the capacitor required by the system is reduced because the DC-link voltage can be regulated by controlling the input power [6]. Various control strategies have been proposed in recent studies on PWM rectifiers given their wide range of applications. Although their principles differ, these strategies can achieve the same main goals, such as low harmonic distorted line current waveforms and high power factor. The most widely known method is voltage-oriented control (VOC) [7], [8], which is based on the current vector orientation with respect to the grid voltage vector. VOC uses two control loops in the *dq* rotating reference frame. The active current is generated to compensate for the DC voltage error by the proportional–integral (PI) controller in the external voltage loop. The active and reactive current errors are reduced by two PI controllers. A space vector modulation (SVM) block is then used to generate gating signals. This control strategy ensures high dynamic and static performance through internal current control loops. However, the final configuration and performance of the VOC system largely depend on the quality of the current control loops. The tuning of PI controllers is also required to ensure system performance under various conditions.

Another high-performance control strategy for the PWM rectifier is direct power control (DPC), which is based on instantaneous active and reactive power control loops [9]-[17]. The conventional switching table-based PDC (ST–DPC) strategy eliminates the need for a current regulator and a modular block. This technique is developed analogously with the direct torque control, which is used in AC-machine drives [9]-[11]. The voltage vector in ST–DPC is selected from a lookup table on the basis of instantaneous active and reactive power errors and grid voltage position [9], [10] or virtual flux position [11]. However, the ST–DPC strategy [12] exhibits two major disadvantages: variable switching frequency and high sampling frequency. To overcome the aforementioned disadvantages [13]-[17], various improved control schemes have been employed. An optimized switching table is developed to reduce power ripples in [13], [14]. DPC–SVM [15]-[17], another control strategy based on

SVM, is analyzed to achieve a constant switching frequency and sinusoidal currents on the AC side with low harmonic distortion.

Predictive control has recently been applied in the control of electrical machines [18]-[20] and power electronics [21]-[23]. Several predictive control strategies have been incorporated with DPC to improve system performance. Predictive DPC can generally be divided into two groups: deadbeat predictive DPC (DPDPC) and model predictive DPC (MPDPC). In DPDPC, the required reference voltage is calculated once in every sampling period by using the system model to reach the reference value in the subsequent sample time [21]. In MPDPC, the system model is used to predict the future behavior of the variables, and a cost function is defined as the criterion to select the optimal voltage vector [22], [23]. This process is different from that of ST–DPC, which selects the voltage vector by using the switching table. Predictive DPC (PDPC) can achieve better steady-state performance and quicker response than DPC.

The aforementioned control strategies for a three-phase PWM rectifier generally require three types of sensors, such as the three voltage/current sensors to measure voltages and currents on the AC side and a DC voltage sensor to measure the DC-link output voltage. In the DPC system, the AC voltage and current are used to calculate the active and reactive powers of the rectifier. To reduce system bulk and complexity and increase system reliability and performance, the use of AC voltage sensors is eliminated [24]-[27]. In [24], the estimation technique for the power source voltage waveforms is applied. However, the calculation of current derivatives can cause operation-related problems. In [25], [26], virtual flux (VF) is introduced in the DPC scheme. The instantaneous active and reactive powers are estimated using the grid VF and AC-side current without the AC-side voltage sensor. The estimation procedures are considerably reliable because no differential operations are involved. In [25] and [26], VF–DPC incorporates the table-based method and the MPDPC approach, respectively.

For a permanent magnet synchronous generator (PMSG)-connected three-phase PWM rectifier used in electromagnetic transmitters, the three-phase input voltages cannot be measured directly. Therefore, this study aims to introduce a model predictive control strategy without the voltage sensor on the AC side for the PMSG-connected PWM rectifier. This method analyzes the relationship among power, back electromotive force (EMF), rotor flux, and convertor voltage. The back EMF used in the prediction is estimated from the historical value of the stator voltage and current. The generator flux is estimated using an equivalent low-pass filter (LPF). Two vectors are employed in a control period. The nonzero vector is selected by a defined cost function, and the zero vector is selected by embracing the principle of deadbeat control to reduce control complexity and computational burden. The simulation and experimental results indicate that the proposed control strategy for the PMSG-connected three-phase PWM rectifiers exhibit better control performance in the power ripple and total harmonic distortion (THD) of line current than the conventional MPDPC-SVM.

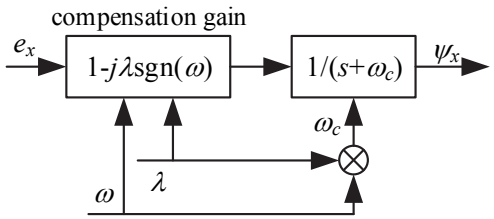

Fig. 6. Flux estimator with compensation.

II. Topology of the Transmitter

An electromagnetic transmitter consists of a diesel generator, PWM rectifier, inverter circuit, and emitter. The topology of the transmitter is illustrated in Fig. 5.

The generator provides the initial power for the transmitter system. The stator windings of the generator and three-phase six-switch circuit comprise the three-phase voltage source PWM converter. In this design, the generator adopts a PMSG or an external-excited generator with a fixed field current. The two types of generators share the same mathematical model. The PWM converter is a crucial component of the design. Compared with a conventional three-phase six-switch voltage-source PWM converter [25], the armature inductance is used as a filter inductor instead of an additional external filter inductor. In practical applications, the high output voltage of the transmitter is usually needed; thus, the boost-type PWM converter is selected. The controllable DC energy of the converter is inverted to a frequency-adjustable square waveform by the inverter circuit, which is transmitted to the ground by the emitting electrode.

III. Predictive Model of the PMSG-Connected PWM Rectifier

A. Machine Equation of the PMSG

PMSG is a strongly coupled and nonlinear system with uncertainty. To obtain the dynamic equation of the PMSG, the following assumptions are made. The field-weakening operation, eddy current, magnetic hysteresis, and magnetic saturation are ignored in this study. The back EMF is supposed sinusoidal.

To prevent complex coordinate transformation, the PMSG model in the $\alpha\beta$ reference frame (stationary reference frame) is preferred. Specifically, the PMSG model can be expressed in the $\alpha\beta$ reference frame by using complex vectors such as [28]

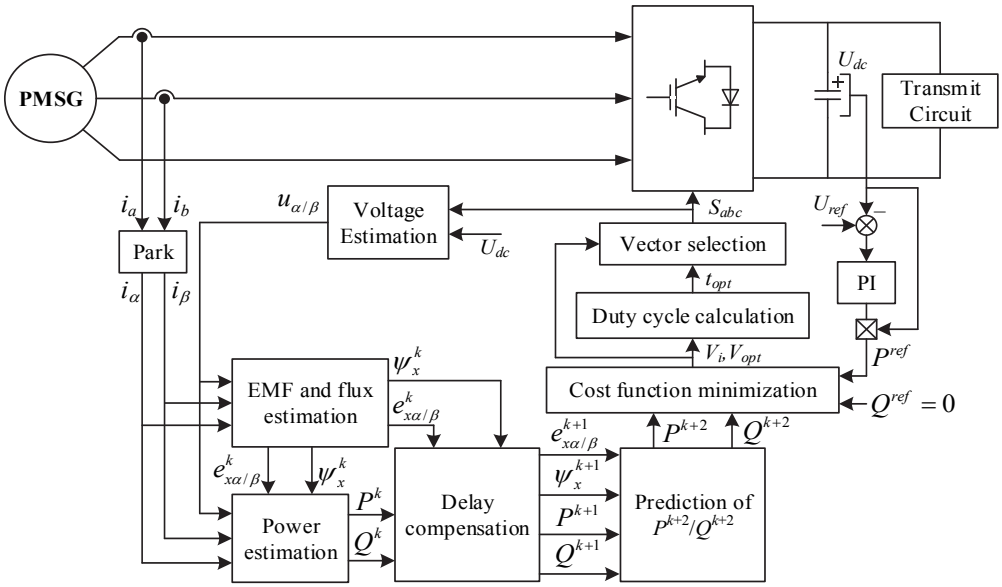

Fig. 7. Control diagram of the proposed MPPC.

$$u_s = -R_s i_s + \frac{d\psi_s}{dt} = -R_s i_s - L_q \frac{di_s}{dt} + \frac{d\psi_x}{dt} = -R_s i_s - L_q \frac{di_s}{dt} + e_x \quad (1)$$

$$\psi_x = [\psi_f - (L_d - L_q) i_d] e^{j\theta_r} , \quad (2)$$

where u_s, i_s, ψ_x, and e_x denote the stator voltage vector, stator current vector, equivalent active flux, and equivalent back EMF, respectively. R_s, ψ_f, L_d, L_q, and θ_r represent the stator resistance, permanent magnet flux, d-axis inductance, q-axis inductance, and electrical rotor position, respectively. i_d is the d-axis current in the synchronous frame.

A surface-mounted PMSG is investigated, and its inductance can be simplified as

$$L_d = L_q = L . \quad (3)$$

In the PMSG–PWM rectifier system, the output voltage of the generator u_s is the input voltage u_{conv} of the PWM rectifier, which can be obtained from the DC-link voltage U_{dc} and the duty cycles of converter switching (D_a, D_b, and D_c), as follows [29]:

$$u_s = u_{conv} = \begin{bmatrix} u_{conv\alpha} \\ u_{conv\beta} \end{bmatrix} = \begin{bmatrix} (\sqrt{2/3}) U_{dc} (D_a - 1/2(D_b + D_c)) \\ (1/\sqrt{2}) U_{dc} (D_b - D_c) \end{bmatrix} . \quad (4)$$

B. Power Estimation

Define

$$\begin{cases} X \otimes Y = \omega(Y_\alpha X_\beta - Y_\beta X_\alpha) \\ X \odot Y = \omega(Y_\alpha X_\alpha + Y_\beta X_\beta) \end{cases} ,$$

where X and Y are the vectors in the $\alpha\beta$ reference frame.

For sinusoidal and balanced back EMF, the instantaneous active power P and reactive power Q in the $\alpha\beta$ reference can be expressed as [29], [30]

$$P = \omega(i_s \otimes \psi_x) = \omega(\psi_{x\alpha} i_\beta - \psi_{x\beta} i_\alpha) , \quad (5)$$

$$Q = \omega(i_s \odot \psi_x) = \omega(\psi_{x\alpha} i_\alpha + \psi_{x\beta} i_\beta) , \quad (6)$$

where ω is the angular velocity of the generator.

The MPDPC is based on time-varying instantaneous power. The power differentiation equation can be obtained from (5) and (6) as follows:

$$\frac{dP}{dt} = \omega(\psi_{x\alpha} \frac{di_\beta}{dt} + \frac{d\psi_{x\alpha}}{dt} i_\beta - \psi_{x\beta} \frac{di_\alpha}{dt} - \frac{d\psi_{x\beta}}{dt} i_\alpha) , \quad (7)$$

$$\frac{dQ}{dt} = \omega(\psi_{x\alpha} \frac{di_\alpha}{dt} + \frac{d\psi_{x\alpha}}{dt} i_\alpha + \psi_{x\beta} \frac{di_\beta}{dt} + \frac{d\psi_{x\beta}}{dt} i_\beta) . \quad (8)$$

The differentiations of $\psi_{x\alpha}$, $\psi_{x\beta}$, i_α, and i_β can be calculated from (1) as follows:

$$\frac{d\psi_{x\alpha}}{dt} = u_{conv\alpha} + R_s i_\alpha + L \frac{di_\alpha}{dt} = e_{x\alpha} , \quad (9)$$

$$\frac{d\psi_{x\beta}}{dt} = u_{conv\beta} + R_s i_\beta + L \frac{di_\beta}{dt} = e_{x\beta} , \quad (10)$$

$$\frac{di_\alpha}{dt} = \frac{1}{L}(e_{x\alpha} - u_{conv\alpha} - R_s i_\alpha) , \quad (11)$$

$$\frac{di_\beta}{dt} = \frac{1}{L}(e_{x\beta} - u_{conv\beta} - R_s i_\beta) . \quad (12)$$

Substituting (9)–(12) into (7) and (8) results in the equations

$$\frac{dP}{dt} = \omega(e_{x\alpha} i_\beta - e_{x\beta} i_\alpha + \frac{\psi_{x\alpha}}{L}(e_{x\beta} - u_{conv\beta} - R_s i_\beta) i_\beta - \frac{\psi_{x\beta}}{L}(e_{x\alpha} - u_{conv\alpha} - R_s i_\alpha)) , \quad (13)$$

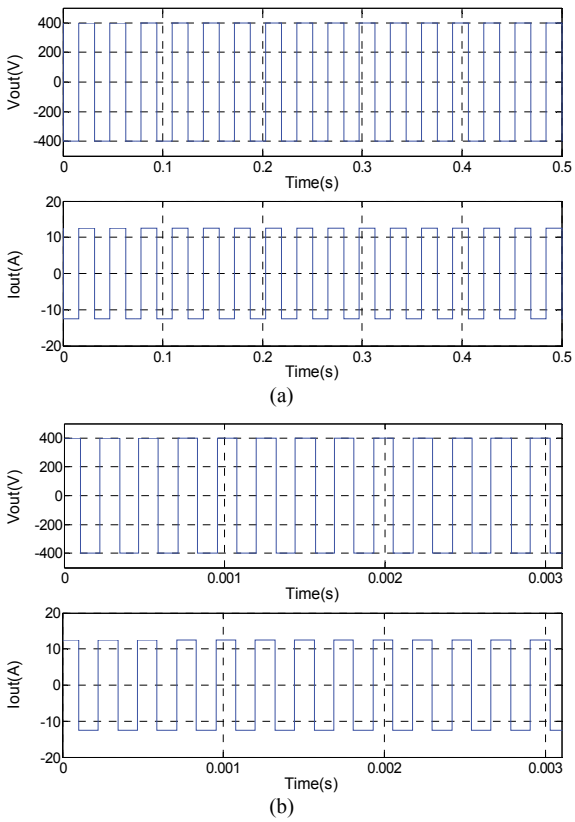

Fig. 8. Output waveforms of the transmitter with different frequencies. (a) 32 Hz. (b) 4096 Hz.

$$\frac{dQ}{dt}=\omega(e_{x\alpha}i_{\alpha}+e_{x\beta}i_{\beta}+\frac{\psi_{x\alpha}}{L}(e_{x\alpha}-u_{conv\alpha}-R_s i_{\alpha})i_{\beta} -\frac{\psi_{x\beta}}{L}(e_{x\beta}-u_{conv\beta}-R_s i_{\beta})) \quad (14)$$

Rearranging (13) and (14) obtains the following equations:

$$\frac{dP}{dt}=\frac{\omega}{L}((\psi_{x\alpha}-Li_{\alpha})e_{x\beta}-(\psi_{x\beta}-Li_{\beta})e_{x\alpha} -(u_{conv}\otimes\psi_x))-\frac{R_s}{L}P \quad (15)$$

$$\frac{dQ}{dt}=\frac{\omega}{L}((\psi_{x\beta}+Li_{\beta})e_{x\beta}+(\psi_{x\alpha}+Li_{\alpha})e_{x\alpha} -(u_{conv}\odot\psi_x))-\frac{R_s}{L}Q \quad (16)$$

From (15) and (16), the active and reactive powers in the next control period can be predicted from the variable at the *k*th instant, as follows:

$$P^{k+1}=P^{k}+t_s[\frac{\omega}{L}((\psi_{x\alpha}-Li_{\alpha})e_{x\beta}-(\psi_{x\beta}-Li_{\beta})e_{x\alpha} -(u_{conv}\otimes\psi_x))-\frac{R_s}{L}P] \quad (17)$$

$$Q^{k+1}=Q^{k}+t_s[\frac{\omega}{L}((\psi_{x\beta}+Li_{\beta})e_{x\beta}+(\psi_{x\alpha}+Li_{\alpha})e_{x\alpha} -(u_{conv}\odot\psi_x))-\frac{R_s}{L}Q] \quad (18)$$

where t_s is the control period.

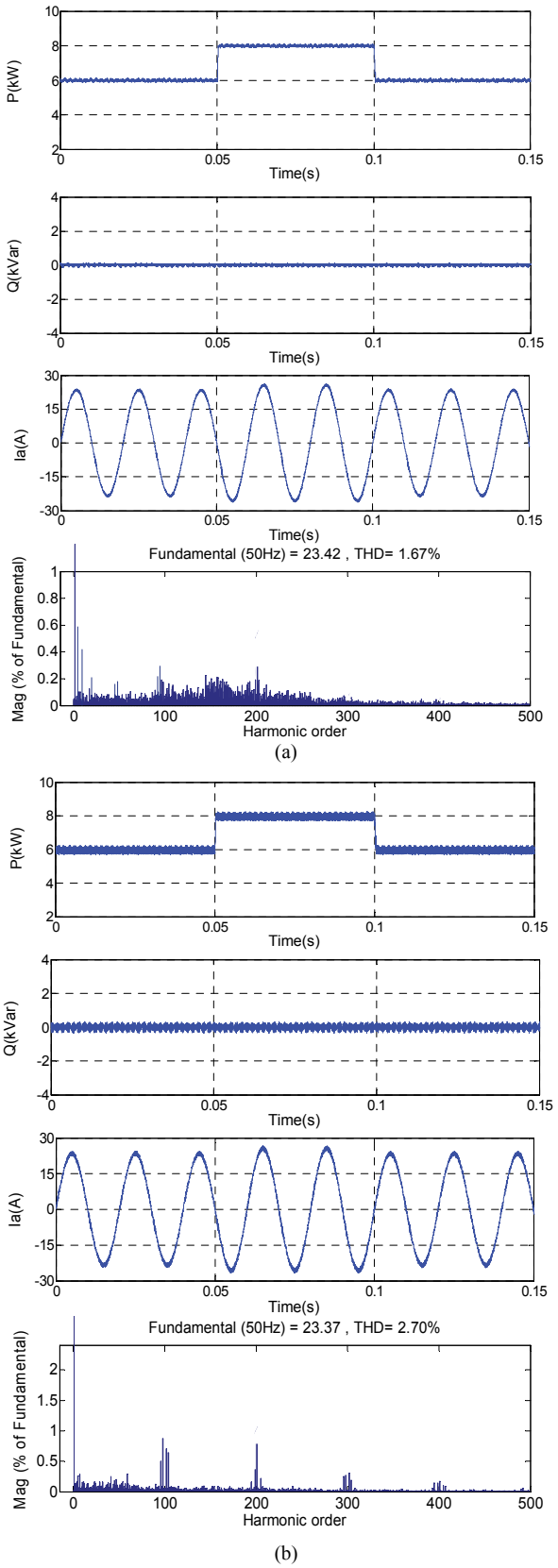

Fig. 9. Response under step change in reference power. (a) Proposed MPDPC. (b) Conventional MPDPC-SVM.

C. EMF Estimation

From (17) and (18), the power can be controlled to a desired value by controlling u_{conv} under the condition that the values of $\psi_{x\alpha}$, $\psi_{x\beta}$, e_α, e_β, i_α, and i_β are determined. The main difficulty in (17) and (18) is that $\psi_{x\alpha}$, $\psi_{x\beta}$, e_α, and e_β cannot be directly measured. Variables e_α and e_β can be calculated using (1) and (2), but the system parameters cannot be precisely determined. In [31, 32], a model-free approach is proposed in which the stator current and the current differences corresponding to different switching states of the rectifier are used to estimate the back EMF. One prior value of the EMF is estimated. However, stability analysis in [31] indicates that the stability region of the estimated inductance ranges from 80% to 125% of the real value. This finding suggests that only approximately 20% error in inductance can be tolerated to maintain system stability. Thus, the proposed algorithm is too sensitive for any practical application. To expand the stability region of the algorithm, the equation order, which is employed to calculate the back EMF, is increased in [28], [31]. The stability region of motor inductance can be significantly broadened to 0%–133% (fourth-order estimator) of inductance variations at the cost of a small increase in computation. The present study adopts the principle applied in [28], [31] by using the mean value of the last two control periods.

From (1), the current equation of the PMSG can be rearranged as

$$\frac{di_s}{dt}=\frac{1}{L}(e_x-u_s-R_s i_s). \tag{19}$$

The prediction of stator current at the (k+1)th instant can be obtained using forward Euler discretization as follows:

$$i_s^{k+1}=i_s^k+\frac{t_s}{L}(e_x^k-u_s^k-R_s i_s^k). \tag{20}$$

For a high-performance PMSG, the rotor speed and back EMF can be generally considered stable; thus, $\omega(k+1)=\omega(k)$, $e_x^k=e_x^{k-1}=e_x^{k-2}$. Considering the variation during one period, the stator current at the kth instant i_s^k can be replaced by $(i_s^k+i_s^{k-1})/2$. In accordance with (20), the EMF at the (k-1)th and (k-2)th instant can be expressed as follows:

$$e_x^{k-1}=u_s^{k-1}-R_s\frac{i_s^k+i_s^{k-1}}{2}-\frac{t_s}{L}(i_s^k-i_s^{k-1}), \tag{21}$$

$$e_x^{k-2}=u_s^{k-2}-R_s\frac{i_s^{k-1}+i_s^{k-2}}{2}-\frac{t_s}{L}(i_s^{k-1}-i_s^{k-2}). \tag{22}$$

The final estimated value of e_x^k is obtained as a mean value of the past EMF, which is expressed as

$$e_x^k=\frac{1}{2}(e_x^{k-1}+e_x^{k-2}). \tag{23}$$

D. EMF Estimation

From (1), the flux ψ_x can be calculated as follows:

$$\psi_x=\int e_x dt. \tag{24}$$

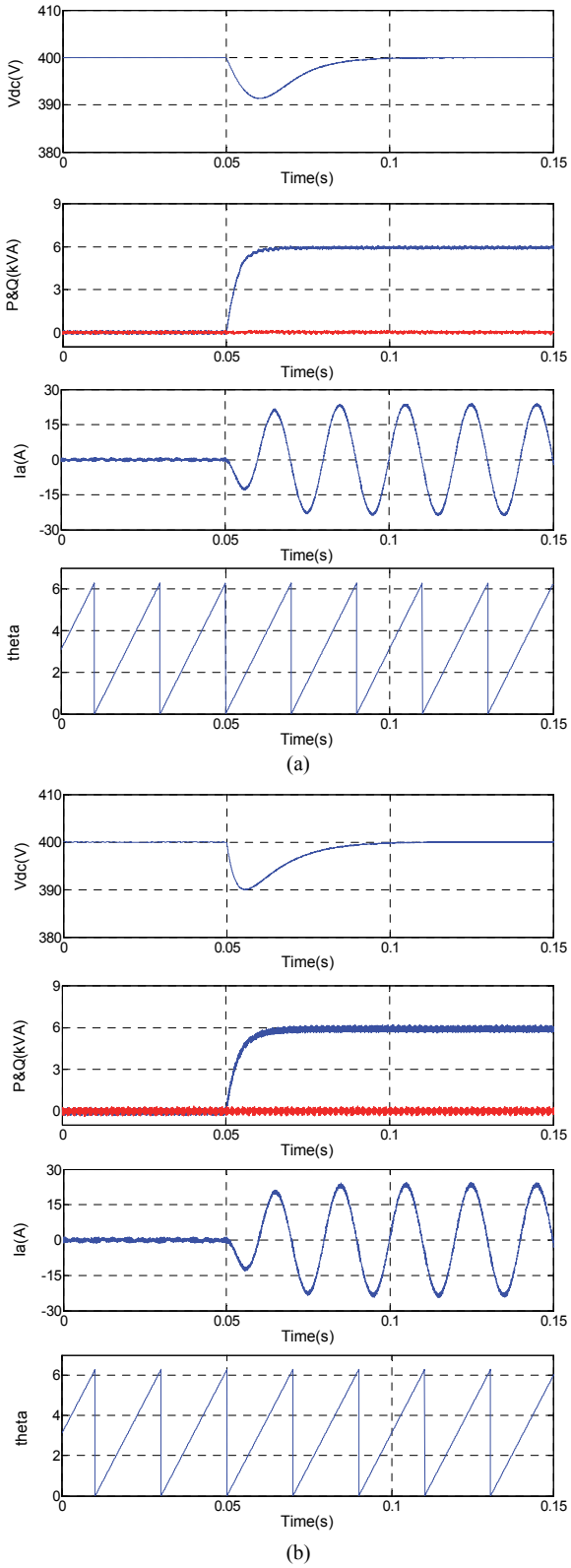

Fig. 10. Response to external sudden load. (a) Proposed MPDPC. (b) Conventional MPDPC-SVM.

This study employs a simple and effective strategy for ψ_x estimation, which is introduced in [33], [34]. By using this method, a high-pass filter is incorporated behind the pure

integration, which is equivalent to a LPF. Thus, drift problems caused by the pure integrator are eliminated. However, an LPF leads to errors in phase and magnitude. Phase lag and magnitude error, respectively, can be expressed as

$$\hat{\phi} = -\tan^{-1}\left(\frac{\omega_c}{\omega}\right), \tag{25}$$

$$\hat{M} = \frac{\sqrt{\omega^2 - \omega_c^2}}{\omega}, \tag{26}$$

where ω_c is the cutoff frequency of the LPF. The gain is compensated for by the gain compensator, and phase lag can be compensated for by the phase compensator. Thus, the new integrator with the phase and gain compensators can be given as

$$\begin{aligned} G(s) &= \frac{1}{s+\omega_c}\frac{\sqrt{\omega^2-\omega_c^2}}{\omega}\exp(\hat{\phi}) \\ &= \frac{1}{s+\omega_c}(1 - j\lambda\,\mathrm{sgn}(\omega)) \end{aligned}. \tag{27}$$

The structure of the ψ_x estimator is shown in Fig. 6, where $\omega_c=\lambda\omega$. The constant λ is typically chosen as λ=0.1 … 0.5. The transient behavior is good if λ is small; however, a high value for λ allows for great DC offset in the measurements. Pure integration is achieved by choosing λ=0. The compensation is conducted before the LPF component to improve the dynamic performance.

IV. Principle of the Proposed MPDPC

In conventional MPDPC, only one control period is selected and applied. Large power ripple occurs as a result of excessive and insufficient control. To achieve a satisfactory steady-state performance, the sample frequency must be high. In this study, the control period is divided into two intervals for two vectors to improve the performance of conventional MPDPC. Thus, a nonzero and a zero vector may be employed during one control period to reduce the power ripple. Fig. 3 presents the overall control diagram of the proposed MPPC. The following parts include vector selection, cost function minimization, and delay compensation.

A. Vector Selection

In conventional DPC, the voltage vector is selected directly from the switching lookup table. In the proposed MPDPC, optimal vectors are selected to minimize the cost function at the end of the next control period. To achieve an effective and accurate vector selection, the cost function is defined and expressed as [25]

$$F = \left(P^{ref} - P^{k+1}\right)^2 + \left(Q^{ref} - Q^{k+1}\right)^2, \tag{28}$$

where the active and reactive powers in the subsequent control period can be calculated from (17) and (18), respectively.

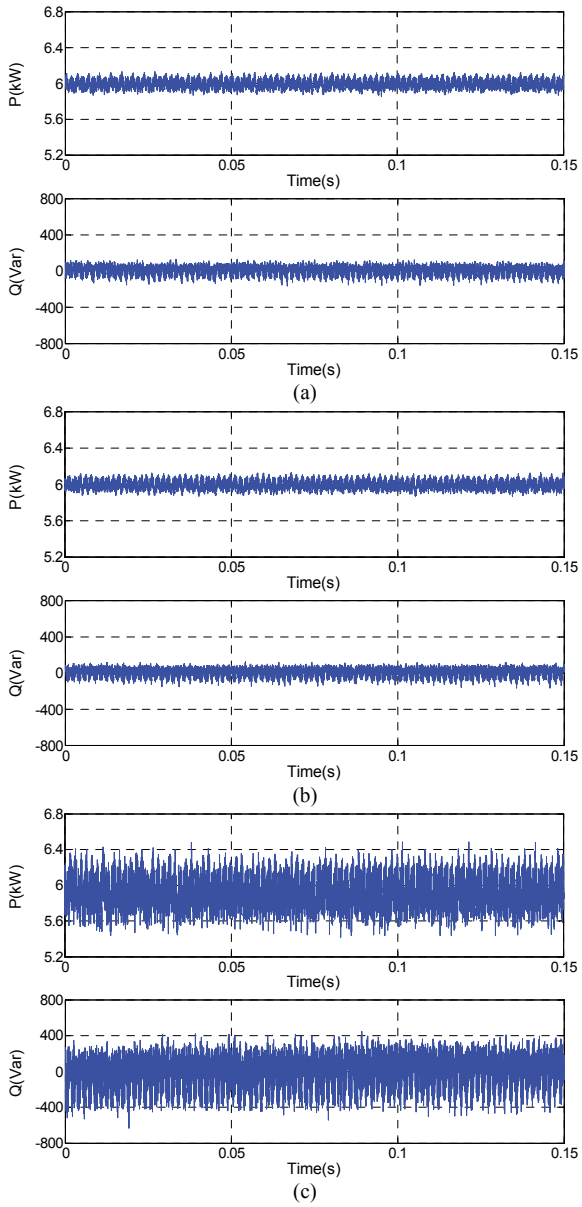

Fig. 11. Simulation results of active and reactive powers when armature inductance differs from real value. (a) L_d=L_q=0.45 mH. (b) L_d=L_q=4.5 mH. (c) L_d=L_q=6 mH.

TABLE I
System Parameters

Parameter	Value
Stator phase resistance	1.14 Ω
Armature inductance	4.5 mH
Flux linkage	0.536 Wb
Pole pairs	2
DC side capacitor	1320 μF
DC side voltage	400 V
Load resistance	32 Ω

To control the operation of the system at unit power factor, the reference value of reactive power is set to zero. Equation (28) can be rewritten as

$$F=\left(P^{ref}-P^{k+1}\right)^2+\left(-Q^{k+1}\right)^2. \quad (29)$$

The best voltage vector minimizing (29) can be selected from eight discrete voltage vectors in the two-level PWM rectifier. If the best vector minimizing (29) is a zero vector, then a suboptimal vector (nonzero vector) should be selected rather than the zero vector.

B. Duty Cycle Calculation

For the MPDPC with duty cycle control, the nonzero vector is selected by evaluating each nonzero vector for (29). The durations of each vector need to be determined after the vector is selected. Suppose that the active power slopes are f_{p1} and f_{p2} for the nonzero and zero vectors, and the reactive power slopes are f_{q1} and f_{q2} for the nonzero and zero vectors, all of which can be obtained using (15) and (16). Equations (30) and (31) determine the linear trajectories of the active and reactive powers under a given nonzero and zero vector application during a control period, as expressed in the following:

$$P^{k+1}=P^k+f_{p1}t_v+f_{p2}(t_s-t_v), \quad (30)$$

$$Q^{k+1}=Q^k+f_{q1}t_v+f_{q2}(t_s-t_v), \quad (31)$$

where t_v is the duration of the nonzero vector and $(t_s–t_v)$ is the duration of the zero vector.

The optimal duration of t_v that minimizes F during a control period satisfies the following condition:

$$\frac{\partial F}{\partial t_v}=0 \quad (32)$$

In solving for (32), the optimal duration t_v for the nonzero vector selected from (29) can be obtained as

$$t_v=\frac{(P^{ref}-P^k)(f_{p1}-f_{p2})+(-q^k)(f_{q1}-f_{q2})}{(f_{p1}-f_{p2})^2+(f_{q1}-f_{q2})^2}+\frac{(t_s-t_v)(f_{p2}^2-f_{p1}f_{p2}-f_{q1}f_{q2}+f_{q2}^2)}{(f_{p1}-f_{p2})^2+(f_{q1}-f_{q2})^2}. \quad (33)$$

C. Delay Compensation

The digital implementation of MPDPC includes a one-step delay between the commanding and applied voltage vectors, a delay that will deteriorate the control performance [22], [35].

In the present study, a one-step delay compensation is employed by predicting the values at the (k+1)th and (k+2)th instants. The variables at the (k+2) instant are used for vector selection and vector durations. The cost function in (29) is rewritten as

$$F=\left(P^{ref}-P^{k+2}\right)^2+\left(-Q^{k+2}\right)^2. \quad (34)$$

In the above equation, P^{k+2} and Q^{k+2} can be predicted as

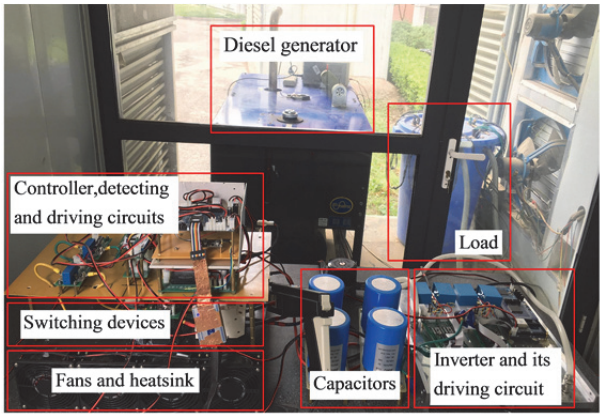

Fig. 12. Experimental setup of electromagnetic transmitter.

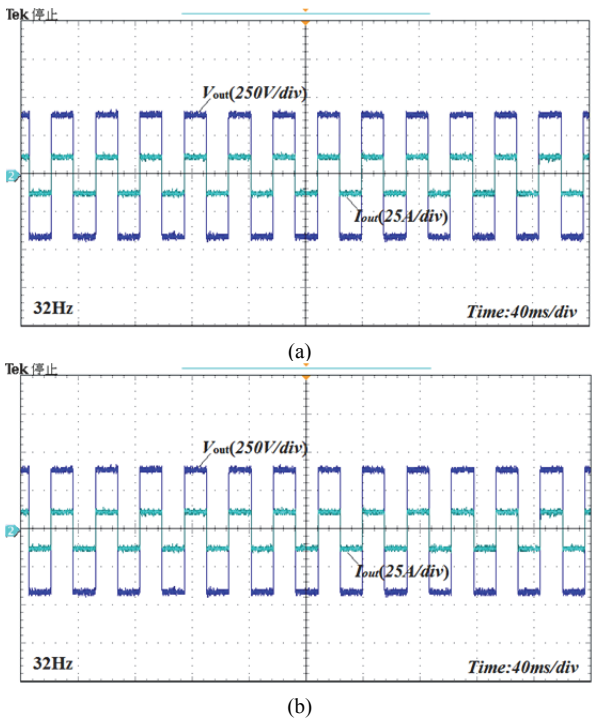

Fig. 13. Experimental output waveforms of the transmitter with different frequencies. (a) 32 Hz. (b) 4096 Hz.

$$P^{k+2}=P^{k+1}+T_s[\frac{\omega}{L}((\psi_{x\alpha}-Li_\alpha)e_{x\beta}-(\psi_{x\beta}-Li_\beta)e_{x\alpha}-(u_{conv}\otimes\psi_x))-\frac{R_s}{L}P]$$

$$Q^{k+2}=Q^{k+1}+T_s[\frac{\omega}{L}((\psi_{x\beta}+Li_\beta)e_{x\beta}+(\psi_{x\alpha}+Li_\alpha)e_{x\alpha}-(u_{conv}\odot\psi_x))-\frac{R_s}{L}Q] \quad (35)$$

where P^{k+1} and Q^{k+1} are predicted using (17) and (18).

V. Simulation and Experimental Results

Fig. 7 illustrates the control diagram of the proposed MPDPC. The three-phase current is transformed into α-axis

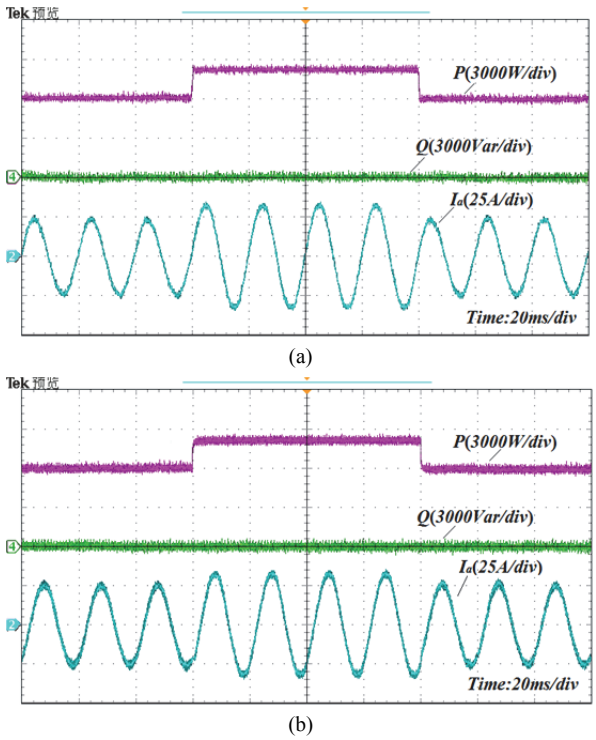

Fig. 14. Experimental results under step change of reference power. (a) Proposed MPDPC. (b) Conventional MPDPC-SVM.

and β-axis currents. The back EMF and flux of the generator are then estimated to calculate the active and reactive powers. The best nonzero and zero vectors are selected by minimizing the cost function (29).

To prove the effectiveness of the proposed control method, a simulation and an experiment are conducted. The results obtained from the conventional MPDPC-SVM are also presented for comparison. In geophysical exploration, the load of the transmitter equals the ground load between the two emission electrodes, which are separated by 1–3 km, and the grounding resistance is nearly 10–80 Ω. In practice, the transmitter needs to provide an excitation current of approximately 10 A. Thus, the present study sets the resistive load at 32 Ω and the output voltage at 400 V. The system control parameters are listed in Table I. To compare the performance of the proposed MPDPC method used in a PMSG-connected PWM rectifier with that of a conventional MPDPC-SVM, the simulation configurations are set under the same condition.

A. Simulation Results

The simulations are carried out in MATLAB/Simulink and the toolbox SimPowerSystem.

For practical electromagnetic prospecting, the transmitter must produce square waveforms at different frequencies. Fig. 8 shows the output waveforms of the transmitter at 32 and 4096 Hz. As shown in the figure, the proposed transmitter can output stable square waveforms with different frequencies to meet practical demands.

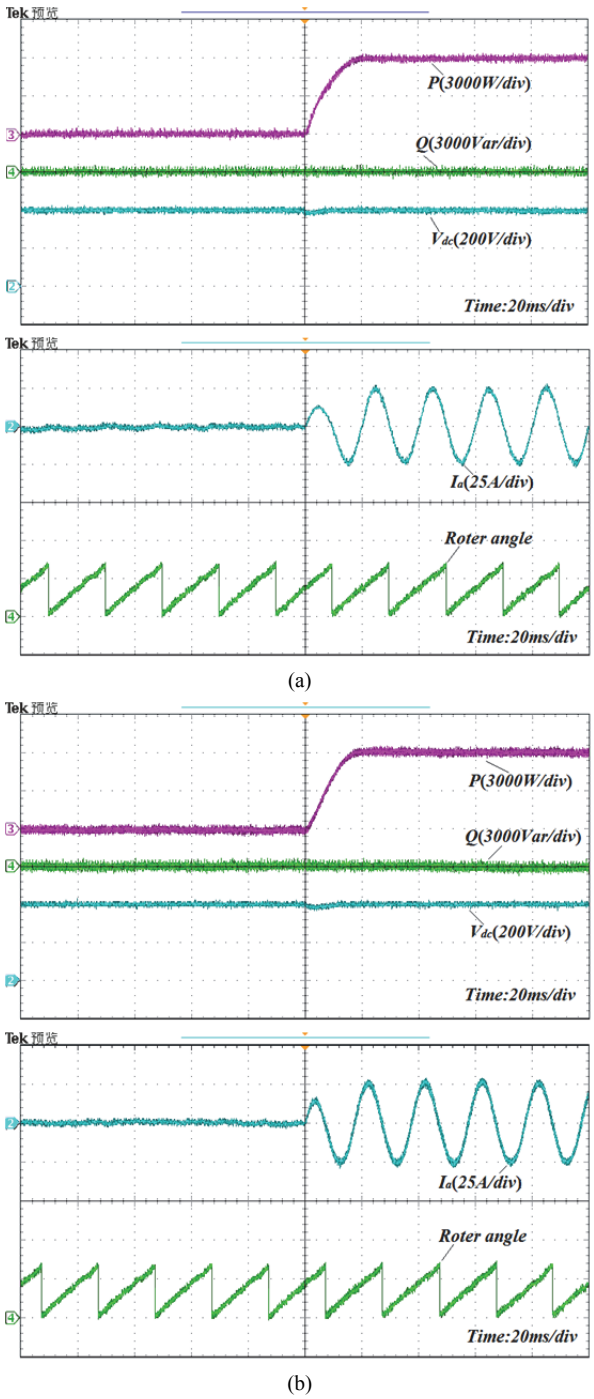

Fig. 15. Experimental results of external sudden load. (a) Proposed MPDPC. (b) Conventional MPDPC-SVM.

In practical application, the grounding resistance in different regions varies from 10 Ω to 80 Ω. However, the resistance variation in one experimental region is within 7 Ω. Therefore, the load resistance in this study is set from 32 Ω to 25 Ω and then back to 32 Ω. The power is varied from 6 kW to 8 kW accordingly. Fig. 9 shows the simulation results under the condition of a step change in active power from 6 kW to 8 kW at t=0.05 s for the proposed MPDPC and the conventional MPDPC-SVM. From top to bottom, the curves

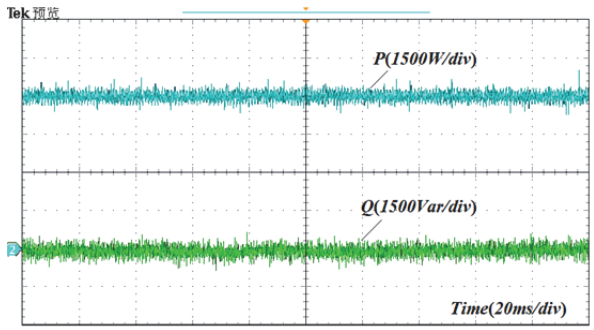

(a)

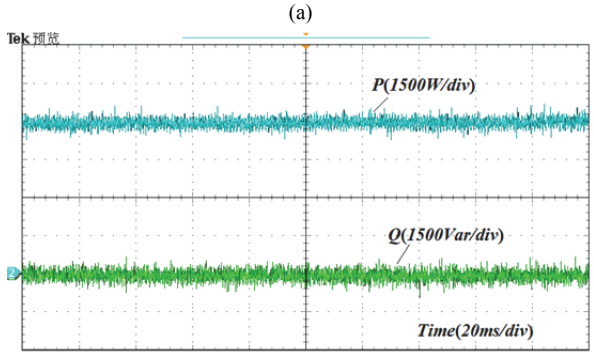

(b)

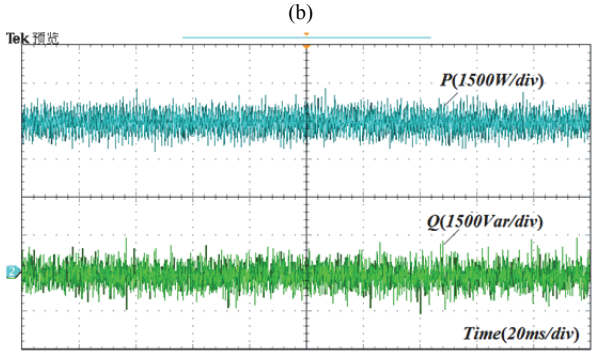

(c)

Fig. 16. Experimental results of active and reactive power when the armature inductance differs from the real value. (a) L_d=L_q=0.45 mH. (b) L_d=L_q=4.5 mH. (c) L_d=L_q=6 mH.

shown are the active power, reactive power, line current, and harmonic spectrum of the line current. As shown in Fig. 9, the active and reactive powers in both control strategies track the reference value quickly without overshoot. However, the power ripples and line current harmonics of the proposed MPDPC are lower than those of the conventional MPDPC-SVM. The THD of the line current is reduced effectively from 2.7% to 1.67%, thus exhibiting excellent line current quality.

Fig. 10 shows the response to an external sudden load for both rectifiers under the same condition of closed DC-link voltage control. From top to bottom, the curves shown are the DC link voltage, active and reactive powers, line currents, and rotor position in Fig. 10. At t=0.05 s, an external load of 32 Ω is applied to the PWM rectifiers. The DC voltage drops slightly and then quickly returns to its reference value, thereby showing strong robustness against load disturbance.

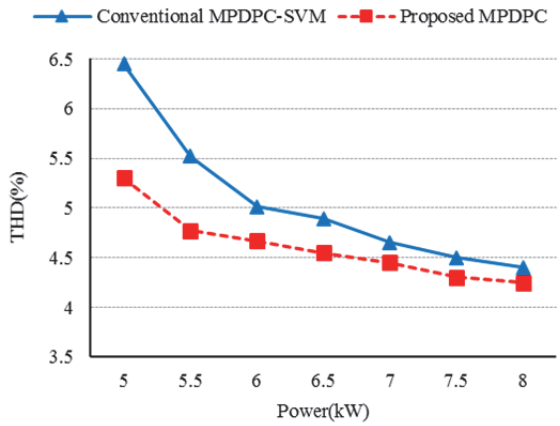

Fig. 17. Line current THD comparison of proposed MPDPC and conventional MPDPC-SVM.

The dynamic process for both methods is similar, but the proposed MPDPC presents less power ripples. Therefore, the proposed control scheme is superior.

To evaluate the robustness of the proposed MPDPC method in the PMSG-connected PWM rectifier, a series of simulations is conducted when the armature inductance differs from the real value (Fig. 11). The figure shows that if the inductance used in the control is 10% of the real value, then the ripples of the active and reactive powers are nearly the same. Meanwhile, if the inductance value used in the control is 133% of the real value, then the ripples of the active and reactive powers increase significantly. The difference in armature inductance (10%–133% of the real value) used for control affects the performance of the control system but not the stability of the system. In [36] and [37], two types of disturbance observers are designed to correct the errors caused by disturbances and uncertainties. To maintain the performance of the proposed MPDPC under different disturbances and uncertainties, a disturbance observer should be used.

B. Experimental Results

The proposed control strategy is verified by a laboratory setup, as shown in Fig. 12. The experimental design includes a diesel generator, a PWM converter with three IGBTs (FF150R12RT4), an inverter circuit with two IGBTs (FF150R12RT4), and a load. A TMS320F28335 control board is employed to implement real-time algorithm coding using C language, and the driving signals are applied to IGBT after going through the driver (CONCEPT 2SD315AI). The driving signals of the PWM converter and inverter circuit are generated by DSP28335 and FPGA (EP2C8Q208C8N), respectively. The parameters of the experimental platform are the same as the simulation parameters.

Figs. 14(a) and 14(b) show the dynamic response of the proposed MPDPC and conventional MPDPC-SVM under the condition of a step change. From top to bottom, the curves are identified as the active and reactive powers and one-phase

current. The active power increases from 6000 W to 8000 W and then decreases to 6000 W. As shown in Fig. 14, the active power quickly tracks the reference value, and the reactive power is controlled to 0 Var to achieve the unit power factor. Both methods achieve decoupling control of the active and reactive powers, and their dynamic performance is highly similar. However, the proposed MPDPC shows lower power ripple and lesser current harmonic than the conventional MPDPC-SVM.

The responses to external sudden load under the condition of closed DC-link voltage are shown in Fig. 15. An external load is suddenly applied to the PWM rectifier, which is similar to the electromagnetic transmitter that starts transmitting power to the ground. From top to bottom, the curves in Fig. 15 are identified as active power, reactive power, DC voltage, one phase current, and rotor angle. The active power is controlled to the reference value, and the reactive power is maintained at 0 Var. The DC-link voltage changes insignificantly during this dynamic process, thereby showing strong robustness against external load disturbance. The dynamic responses of both methods are highly similar.

Fig. 16 presents the experimental results when the generator armature inductance value in the calculation is different from the actual armature inductance value (4.5 mH). As shown in Figs. 16(a) and 16(b), if the armature inductance value used in the control is 10% of the real value (0.45 mH), then the ripples of active and reactive powers are the same as the real value. Meanwhile, if the value used in the control is 133% of the real value (6 mH), then the ripples of the active and reactive powers increase significantly, as shown in Fig. 16(c), but the unit power factor is maintained. Overall, when the value of armature inductance varies from 10% to 133% of the real value, the proposed algorithm remains stable and controllable.

A comparison of both control methods in terms of the THD of the line current is shown in Fig. 17. In general, the THD of the line current for the proposed MPDPC is lower than that of the conventional method in different power regions.

VI. CONCLUSIONS

An MPDPC PMSG-connected PWM rectifier used in electromagnetic transmitters is proposed in this study. Different from the conventional grid-connect PWM rectifier, in which three external inductances are connected in series with the grid and the rectifier, the proposed PWM rectifier directly connects with the generator, which will make the transmitter small in size and light in weight. The armature inductance of the generator is used as the filter inductance. A power dynamic equation is developed for the analysis of the real-time power behavior. In MPDPC, a nonzero vector and a zero vector are applied in one control period. To select the optimal vector and calculate the duration of the vector, a cost function is predefined. Simulation and experimental results demonstrate that the proposed PMSG-connected PWM rectifier used in electromagnetic transmitters can meet the requirements of geophysical exploration. Moreover, compared with the conventional MPDPC-SVM, the proposed MPDPC effectively improves power ripples and line current harmonics.

ACKNOWLEDGMENT

This work was supported by the National Key Research and Development Plan under Grant No. 2016YFC0303103.

REFERENCES

[1] Q. Y. Jiang, "Study on the key technology of wide field electromagnetic sounding instrument," Ph.D. Thesis, Central South University, Changsha, China, 2010.

[2] K. Xue, S. Wang, J. Lin, G. Li, and F. Zhou, "Loss analysis and air-cooled design for a cascaded electrical source transmitter," *J. Power Electron.*, Vol. 12, No. 5, pp. 530-543, Mar. 2015.

[3] F. Yu and Y. Zhang, "Modeling and control method for high-power electromagnetic transmitter power supplies," *J. Power Electron.*, Vol. 13, No. 4, pp. 679-691, Jul. 2013.

[4] Q. Zhen, Q. Di, and H. Liu, "Key technology study on CSAMT transmitter with excitation control," *Chinese J. Geophysics,* Vol. 56, No. 11, pp. 3751-3760, Nov. 2013.

[5] X. Z. Zhu, "Based on the soft switch technology research and implementation of high-power electromagnetic transmitter," Master Thesis, Beijing University of Technology, Beijing, China, 2016.

[6] J. R. Rodríguez, J. W. Dixon, J. R. Espinoza, J. Pontt, and P. Lezana, "PWM regenerative rectifiers: State of the art," *IEEE Trans. Ind. Electron.*, Vol. 52, No. 1, pp. 5-22, Feb. 2005.

[7] B. Yin, R. Oruganti, S. K. Panda, and A. K. Bhat, "An output-power-control strategy for a three-phase PWM rectifier under unbalanced supply conditions," *IEEE Trans. Ind. Electron.*, Vol. 55, No. 5, pp. 2140-2151, May 2008.

[8] X. H. Wu, S. K. Panda, and J. X. Xu, "DC link voltage and supply-side current harmonicsminimization of three phase PWM boostrectifiers using frequency domain based repetitive current controllers," *IEEE Trans. Power Electron.*, Vol. 23, No. 4, pp. 1987-1997, Jul. 2008.

[9] T. Noguchi, H. Tomiki, S. Kondo, and I. Takahashi, "Direct power control of PWM converter without power-source voltage sensors," *IEEE Trans. Ind. Appl.*, Vol. 34, No. 3, pp. 473-479, May/Jun. 1998.

[10] G. Escobar, A. M. Stankovic, J. M. Carrasco, E. Galvan, and R. Ortega, "Analysis and design of direct power control (DPC) for a three phase synchronous rectifier via output regulation subspaces," *IEEE Trans. Power Electron.*, Vol. 18, No. 3, pp. 823-830, May 2003.

[11] M. Malinowski, M. P. Kazmierkowski, S. Hansen, F. Blaabjerg, and G. D. Marques, "Virtual-flux-based direct power control of three-phase PWM rectifiers," *IEEE Trans. Ind. Appl.*, Vol. 37, No. 4, pp. 1019-1027, Jul./Aug. 2001.

[12] Y. Zhang, Z Li, Y. Zhang, W. Xie, Z. Piao, and C. Hu, "Performance improvement of direct power control of

PWM rectifier with simple calculation," *IEEE Trans. Power Electron.*, Vol. 28, No. 7, pp. 3428-3437, Jul. 2013.
[13] A. M. Razali, M. A. Rahman, G. George, and A. R. Nasrudin, "Analysis and design of new switching lookup table for virtual flux direct power control of grid-connected three-phase PWM AC–DC converter," *IEEE Trans. Ind. Appl.*, Vol. 51, No. 2, pp. 1189-1200, Mar./Apr. 2015.
[14] A. Bouafia, F. Krim, and J. P. Gaubert, "Fuzzy-logic-based switching state selection for direct power control of three-phase PWM rectifier," *IEEE Trans. Ind. Electron.*, Vol. 56, No. 6, pp. 1984-1992, Jun. 2009.
[15] J. A. Restrepo, J. M. Aller, J. C. Viola, A. Bueno, and T. G. Habetler, "Optimum space vector computation technique for direct power control," *IEEE Trans. Power Electron.*, Vol. 24, No. 6, pp. 1637-1645, Jun. 2009.
[16] M. Malinowski, M. Jasinski, and M. P.Kazmierkowski, "Simple direct power control of three-phase PWM rectifier using space-vector modulation (DPC-SVM)," *IEEE Trans. Ind. Electron.*, Vol. 51, No. 2, pp. 447-454, Apr. 2009.
[17] J. Restrepo, J. Viola, J. M. Aller, and A. Bueno, "A simple switch selection state for SVM direct power control," in *Proc. ISIE*, pp. 1112-1116, 2006.
[18] T. Geyer, G. Papafotiou, and M. Morari, "Model predictive direct torque control – Part I: Concept, algorithm, and analysis," *IEEE Trans. Ind. Electron.*, Vol. 56, No. 6, pp. 1894-1905, Jun. 2009.
[19] M. Preindl and S.Bolognani, "Model predictive direct torque control with finite control set for PMSM drive systems, part 2: Field weakening operation," *IEEE Trans. Ind. Inform.*, Vol. 9, No. 2, pp. 648-657, May. 2013.
[20] M. Pacas, J. Weber, "Predictive direct torque control for the PM synchronous machine," *IEEE Trans. Ind. Electron.*, Vol. 52, No. 5, pp. 1350-1356, Oct. 2005.
[21] A. Bouafia, J. P. Gaubert, and F. Krim, "Predictive direct power control of three-phase pulsewidth modulation (PWM) rectifier using space-vector modulation (SVM)," *IEEE Trans. Power Electron.*, Vol. 25, No. 1, pp. 228-236, Jan. 2010.
[22] P. Cortes, J. Rodriguez, P. Antoniewicz, and M. Kazmierkowski, "Direct power control of an AFE using predictive control," *IEEE Trans. Power Electron.*, Vol. 23, No. 5, pp. 2516-2523, Jan. 2008.
[23] D. E. Quevedo, R. P. Aguilera, M. A. Pérez, P. Cortes, and R. Lizana, "Model predictive control of an AFE rectifier with dynamic references," *IEEE Trans. Power Electron.*, Vol. 27, No. 7, pp. 3128-3136, Jul. 2012.
[24] J. G. Norniella, J. M. Cano, G. A. Orcajo, C. H. R. Garcia, J. F. Pedrayes, M. F. Cabanas, and M. G. Melero, "Analytic and iterative algorithms for online estimation of coupling inductance in direct power control of three-phase active rectifiers," *IEEE Trans. Power Electron.*, Vol. 26, No. 11, pp. 3298-3307, Nov. 2011.
[25] A. M. Razali, M. A. Rahman, G. George, and N. A. Rahim, "Analysis and design of new switching lookup table for virtual flux direct power control of grid-connected three-phase PWM AC–DC converter," *IEEE Trans. Ind. Appl.*, Vol. 51, No. 2, pp. 1189-1200, Mar./Apr. 2015.
[26] Y. Cho and K. B. Lee, "Virtual-flux-based predictive direct power control of three-phase PWM rectifiers with fast dynamic response," *IEEE Trans. Power Electron.*, Vol. 31, No. 4, pp. 3348-3359, Apr. 2016.
[27] Y. Zhang, W. Xie, Z. Li, and Y. Zhang, "Model predictive direct power control of a PWM rectifier with duty cycle optimization," *IEEE Trans. Power Electron.*, Vol. 28, No. 11, pp. 5343-5351, Nov. 2013.
[28] Y. Zhang, D. Xu, J. Liu, S. Gao, and W. Xue, "Performance improvement of model predictive current control of permanent magnet synchronous motor drives," *IEEE Trans. Ind. Appl.*, Vol. 53, No. 4, pp. 3683-3695, Jul./Aug. 2017.
[29] P. Antoniewicz and M. P. Kazmierkowski, "Virtual-flux-based predictive direct power control of AC/DC converters with online inductance estimation," *IEEE Trans. Ind. Electron.*, Vol. 55, No. 12, pp. 4381-4390, Dec. 2008.
[30] D. Zhi, L. Xu, and B. W. Williams, "Improved direct power control of grid-connected DC/AC converters," *IEEE Trans. Power Electron.*, Vol. 24, No. 5, pp. 1280-1292, May 2009.
[31] C. K. Lin, T. H. Liu, L. C. Fu, and C. F. Hsiao, "Model-free predictive current control for interior permanent-magnet synchronous motor drives based on current difference detection technique," *IEEE Trans. Ind. Electron.*, Vol. 61, No. 2, pp. 667-681, Feb. 2014.
[32] W. Wang and X. Xi, "Current control method for PMSM with high dynamic performance," in *Conf. IEMDC*, pp. 1249-1254, 2013.
[33] M. H. Shin, D. S. Hyun, S. B. Cho, and S. Y. Choe, "An improved stator flux estimation for speed sensorless stator flux orientation control of induction motors," *IEEE Trans. Power Electron.*, Vol. 15, No. 2, pp. 312-318, Mar. 2000.
[34] M. Hinkkanen and J. Luomi, "Modified integrator for voltage model flux estimation of induction motors," *IEEE Trans. Ind. Electron.*, Vol. 50, No. 4, pp. 818-820, Aug. 2003.
[35] P. Cortes, J. Rodriguez, C. Silva, and A. Flores, "Delay compensation in model predictive current control of a three-phase inverter," *IEEE Trans. Ind. Electron.*, Vol. 59, No. 2, pp. 1323-1325, Feb. 2012.
[36] J. Yang, H. Cui, S. Li, and A. Zolotas, "Optimized active disturbance rejection control for DC-DC buck converters with uncertainties using a reduced-order GPI observer," *IEEE Trans. Circuits Syst. I, Reg. Papers*, Vol. 65, No. 2, pp. 832-841, Feb. 2018.
[37] J. Yang, W. Zheng, S. Li, B. Wu, and M. Cheng, "Design of a prediction-accuracy-enhanced continuous-time MPC for distuibed systems via a disturbance observer," *IEEE Trans. Ind. Electron.*, Vol. 62, No. 9, pp. 5807-5816, Sep. 2015.

Jialin Zhang was born in Hebei, China, in 1990. He received his B.S. degree from the School of Electrical Engineering, Hebei University of Science and Technology, Hebei, China, in 2012; and his M.S. degree from the College of Information Science and Engineering, Northeastern University, Liaoning, China, in 2014. He is currently working toward his Ph.D. degree in the Faculty of Information, Beijing University of Technology, Beijing, China. His current research interests include control of pulse width modulation rectifier connected with permanent synchronous generator and its application in geophysics.

Yiming Zhang was born in Hubei, China, in 1964. He received his B.S. degree from the School of Electronic, Information and Electrical Engineering, Shanghai Jiao Tong University, Shanghai, China, in 1988; and his M.S. degree from the School of Electrical Engineering and Automation, Harbin Institute of Technology, Harbin, China, in 1992. From 2000 to 2007, he was a senior researcher in the Institute of Electrical Engineering, Chinese Academy of Sciences, Beijing, China. Since 2008, he has been a professor in the College of Electronic Information and Control Engineering, Beijing University of Technology, Beijing, China. His current research interests include intelligent power management, motor speed control, servo drivers, and motor energy conservation.

Bing Guo was born in Hebei, China, in 1990. He received the B.S. degree in Electronic Information Engineering from Shijiazhang Tiedao University, Hebei, China, in 2011; and his M.S. degree in Control Science and Engineering from Beijing University of Technology, Beijing, China, in 2014. He is currently studying for a doctor's degree in power electronics and geophysical prospecting at Beijing University of Technology.

Junxia Gao was born in Tianjin, China, in 1978. She received her B.S. degree from the College Information Engineering, Taiyuan University of Technology, Taiyuan, China, in 2001; and her M.S. degree from the Faculty of Information, Beijing University of Technology, Beijing, China, in 2004. Since 2004, she has been a senior lecturer in the Faculty of Information, Beijing University of Technology. Her current research interests include power electronics, electromagnetic fields, and nondestructive examination.